DEVELOPMENT AND EVALUATION OF STRATEGIES FOR PARALLEL OPERATION OF FUEL CELL STACKS

S. Nicolay*‡, L. Fritsche‡, S. Lück‡, J. Friedrichs‡, R. Doering*

* MTU Aero Engines AG, Flying Fuel Cell, Dachauer Str. 665, München, DE

‡ Technische Universität Braunschweig, Institut für Flugantriebe und Strömungsmaschinen, Hermann- Blenk-Straße 37, Braunschweig, DE

Abstract

This paper describes the modeling of a fuel cell system, a model-based development of corresponding automation strategies, and an experimental evaluation of the model and automation on a scaled system test rig. The developed system model includes the fuel cell stack and associated peripheral components such as air blowers and valves. The focus of the modeling is laid on transient effects and, in particular, the influences of stack temperature, partial pressures and humidities of the reaction gases on the voltage characteristics of the stacks. The automation strategy developed in the subsequent step includes control of hydrogen pressure, air ratio and coolant temperature using PI controllers. The automation strategy also includes a superordinate state machine for controlling and monitoring the entire system. The automation strategy is evaluated experimentally on two stacks which are electrically interconnected in parallel. The challenge of an unequal current distribution between fuel cell stacks due to different stack performances is also addressed. In order to be able to react to larger load changes and to failure cases, the switching on and off of an entire stack during operation is also investigated and evaluated for the parallel interconnection.

Keywords

fuel cell; hydrogen; aircraft propulsion; electric flight, modeling, control design

Supported by:

Federal Ministry for Economic Affairs and Climate Action

on the basis of a decision by the German Bundestag

NOMENCLATURE

Symbols

α	charge transfer coefficient	-
A	area	m^2
ρ	density	kg/m^3
d_m	membrane thickness	cm
E	Nernst potential	V
E_c	activation energy	J/mol
F	Faraday constant	C/mol
γ	pressure coefficient	-
h	enthalpy	J
I	current	A
i	current density	A/cm^2
i_0	exchange current density	A/cm^2
i_n	leakage current density	A/cm^2
K	pressure drop coefficient	various
k	heat transfer coefficient	W/(m^2 K)
k_s	static gain	various
K_v	flow factor	m^3/h
L	characteristic length	m
λ	air ratio	-
λ_m	membrane water content	-
μ	dynamic viscosity	Pa s
M	molar mass	kg/mol
$\dot{m}$	mass flow rate	kg/s

doi: 10.25967/570412

N	number of cells	-
p	pressure	Pa
$\dot{Q}$	Heat flow rate	W
R	resistance	Ohm cm^2
R	universal gas constant	J/(mol K)
σ	electric conductivity	$(\Omega \cdot \mathrm{cm})^{-1}$
T	temperature	K
t	time	s
τ	time constant	s
U	voltage	V

Indices

act	activation loss
dem	demand
lam	laminar
m	membrane
ref	reference value
trans	transportation loss
turb	turbulent

Abbreviations

DC	direct current
expt	experiment
sim	simulation

1. INTRODUCTION

The aviation industry is seeking to drastically reduce its emissions. Especially the engine manufacturers want to provide alternative, emission-free propulsion systems. Research institutes and industry are collaborating closely to investigate different more environmentally friendly propulsion concepts. In this context, electric propulsion systems have gained great attention. However, energy storage systems for electric energy must be considered wisely with respect to properties such as energy capacity or weight. One promising energy storage for electric propulsion is given by hydrogen. The chemical energy of hydrogen can be converted on board to electric energy using fuel cells. The electric energy in turn can be used to power an electric motor.

Compared to other mobile fuel cell applications, e.g. automotive, the power demand of passenger aircraft is much higher (> 1 MW [1]). However, fuel cell stacks cannot be built to any size due to structural and other reasons [2]. Consequently, the total power demand must be divided into several fuel cell stacks. These stacks must then be electrically interconnected to provide the full required electric power. Both serial and parallel interconnection of stacks can be considered. However, the serial interconnection leads to high voltages which bring the risk of static discharge [3]. Parallel interconnection of fuel cell stacks, on the other hand, may be a promising approach to enable a large electric power supply.

In order to investigate parallel interconnection of fuel cell stacks, a scaled system test rig is built including necessary peripheral system components such as valves, air blowers and heat exchangers. A schematic of the investigated fuel cell system is depicted in Figure 1. The shown system is doubled and the two stacks are interconnected electrically. The investigation further requires a suitable automation strategy including control of the peripheral system components to set the operating conditions of the stacks. The automation strategy and controls are developed based on a physical system model which represents the above-mentioned test rig.

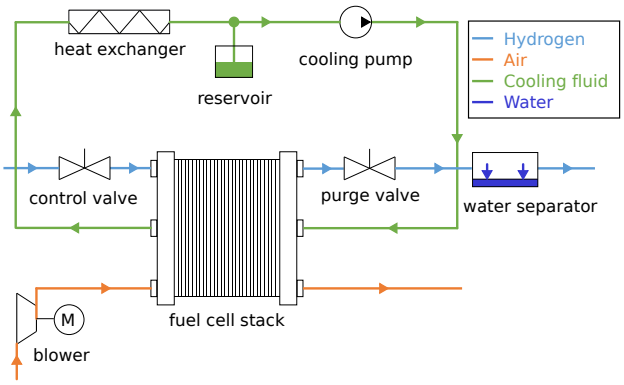

FIG 1. Schematic of the investigated fuel cell system

The presented work has the following structure. A general discussion of serial and parallel stack interconnection and its individual advantages and disadvantages is given in section 2. Following, the test rig used to investigate the stack interconnection is described in more detail in section 3. The physical system model representing the test rig is described subsequently in section 4 and the developed automation strategy is outlined in section 5. At last, the automation strategy is transferred to the test rig. In section 6 experimental data will first be used to validate parts of the system model before eventually the results of the stack interconnection will be discussed in detail.

2. ELECTRICAL INTERCONNECTION OF FUEL CELL STACKS

A PEM fuel cell stack is limited in size both in terms of structure and with regard to the desired uniform distribution of operating conditions within the stack. For example, large bipolar plates can lead to a more uneven distribution of operating conditions. Large cell numbers, on the other hand, can lead to problems

when compressing the stack and long distribution channels along the stack lead to large pressure drops. [2]

To increase the performance of a fuel cell system and thus provide high electric power, multiple fuel cell stacks can be electrically interconnected. For the interconnection of several stacks to a fuel cell module, parallel and series connection are possible and will be described below.

Serial interconnection

The serial connection is the simpler way to connect several fuel cell stacks to achieve a desired power level. The basic behavior of fuel cell stacks connected in series is similar to the operation of single stacks. The current through the fuel cell stacks is the same, while the voltages of the stacks add up. For two stacks, this results in a total voltage $U_{\text{total, serial}}$ that is theoretically twice as high as in the parallel connection (cf. Equation 1) while the current remains the same (cf. Equation 2). Such high voltages at low currents lead to lower heat generation in the electrical conductors. However, high DC voltages also bring the risk of damaging static discharge [3]. Furthermore, a lot of electrical components in aviation are built according to the MIL-STD-704F [4] standard of 270 V DC, so higher voltages may be unpractical when considering the overall system architecture. The basic structure of the serial interconnection is shown in Figure 2a).

(1) $$U_{\text{total, serial}} = U_{\text{stack}_1} + U_{\text{stack}_2} + U_{\text{stack}_n}$$

(2) $$I_{\text{total, serial}} = I_{\text{stack}_1} = I_{\text{stack}_2} = I_{\text{stack}_n}$$

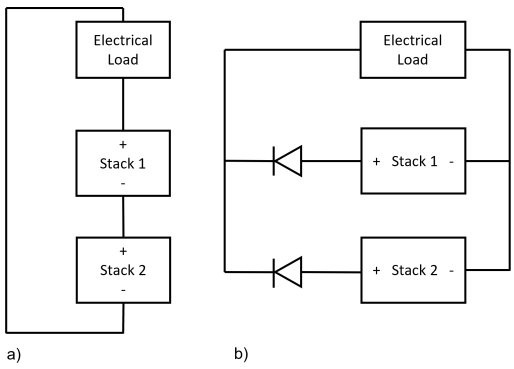

FIG 2. Schematic of the a) serial and b) parallel interconnection of fuel cell stacks

Parallel interconnection

Another way to achieve a desired power level is to connect several fuel cell stacks in parallel as shown in Figure 2b). In contrast to the series connection, within a parallel connection the currents add up according to Equation 3, while the voltage provided by the stacks is identical (cf. Equation 4).

(3) $$I_{\text{total, parallel}} = I_{\text{stack}_1} + I_{\text{stack}_2} + I_{\text{stack}_n}$$

(4) $$U_{\text{total, parallel}} = U_{\text{stack}_1} = U_{\text{stack}_2} = U_{\text{stack}_n}$$

The challenge with the electrical interconnection of several fuel cell stacks in parallel is the fact that each fuel cell stack can have different performance characteristics due to different operating conditions, manufacturing tolerances or degradation effects. When looking at the polarization curves in Figure 3, it becomes clear that the stacks, in case of different power behaviors, deliver different currents at the same voltage. This can lead to significantly different operating points. It can happen that one of the stacks supplies the maximum permissible current much earlier than the other stack, which on the one hand causes high heat generation and on the other hand may lead to irreversible degradation of the stack. To avoid this, monitoring of the individual parameters of each fuel cell stack is necessary. Furthermore, the difference in current between the two stacks at the same voltage can cause a reverse current into one of the stacks. To avoid such a reverse current, a Schottky diode should be installed behind each stack in such configurations.

Precise control of the peripheral system components might be a suitable measure to create nearly equal operating conditions for all stacks, enabling parallel interconnection. Hence, the goal of the presented work is to develop such automation strategies, as described in detail in section 5.

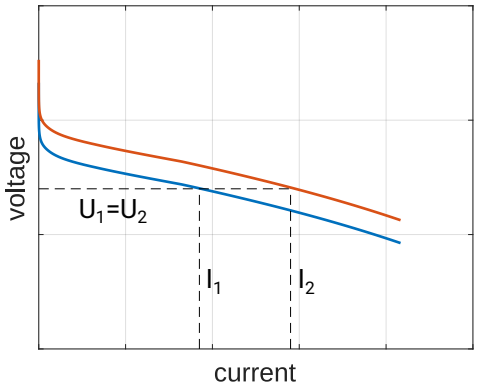

FIG 3. Theoretical polarization curves of two stacks with different performances. The current divides unequally.

3. FUEL CELL SYSTEM TEST RIG

Since a fuel cell system in the power class of an aircraft engine is very complex and expensive, a scaled system is considered in this work. This allows for quick and cost-effective experimental studies. The fuel cell system test rig contains the most important components that can be found in a more powerful

system and is therefore suitable to validate the automation approaches developed for parallel stack operation. The test rig is made up of two individual systems, each of which contains the components shown in Figure 1. The peripheral components are completely independent for both systems, so that the fuel cell systems are only connected to each other via the electrical connection of the stacks. The peripheral components, such as the compressor and the valves are controlled for both systems individually according to the control approaches described in section 5.

The peripherals can be categorized into three subsystems. The hydrogen subsystem, the air subsystem and the coolant subsystem. In the hydrogen subsystem, the hydrogen is supplied via a pressurized tank with a reduced pressure of about 4 bar at the test rig inlet. This is then regulated to a constant pressure via a pressure control valve at the anode inlet. A further valve is installed at the anode outlet, which can be opened for short periods at regular intervals to remove residual gases and product water from the flow field channels. In the air subsystem, atmospheric air is supplied to the fuel cell stack on the cathode side via a compressor in order to provide the oxygen required for the reaction. The operating temperature of the fuel cell stack is adjusted via the coolant subsystem. This consists of a coolant pump and a heat exchanger, which has two axial fans.

4. MODELING OF A FUEL CELL SYSTEM

A physical model of the fuel cell system is developed as a basis for further investigations as well as for the control design. Therefore, a special focus is laid on the modeling of the transient system behavior. The model shall hence be able to describe
1) the gas dynamics in the system,
2) thermal effects and
3) the humidities of the reactant gases.

A physical network modeling approach, provided by Matlab Simscape [5], is chosen to meet these requirements. Thereby, each system component is described via physical or semi-empirical algebraic or differential equations. The interconnection of the individual components leads to a differential-algebraic system of equations (DAE) which is solved numerically. The most important equations used to model the fuel cell system components comprise mainly algebraic equations and will be described below. Differential equations describing pressure, temperature and humdidity dynamics are already implemented in the according Matlab Simscape standard components (cf. e.g. [6]).

4.1. Modeling of the fuel cell stack

The fuel cell stack model comprises a fluid model describing the mass flow and pressure losses within the hydrogen and air flow fields, a voltage model which describes the fuel cell stack voltage as a function of the current demand and a thermal model describing the distribution of reaction heat within the stack. Models similar to the one developped here can be found in [7], [8], [9] or [10]. A schematic of the fuel cell stack model is shown in the appendix in Figure 13.

Fluid model

The fuel cell stack's fluid model consists of constant volume chambers representing the hydrogen and air flow field volumes, respectively, and pressure loss elements, one before and one after the volume chambers, as depicted exemplarily for the cathode in Figure 4. Laminar flow is assumed for both reactant gases. The differential pressure loss Δp is described according to [11]:

$$\Delta p = \frac{8\pi\mu L\dot{V}}{A^2} \tag{5}$$

where μ is the dynamic viscosity, L is the characteristic length of the flow field, $\dot{V}$ is the volumetric flow rate and A, as an approximation, is the sum of the cross-sectional areas of the flow field channels. The characteristic length L is calculated from a reference volumetric flow rate and the associated pressure loss.

The fluid model further accounts for reactant gas consumption and water production. Consumption and reaction rates are described as a function of the current demand in Equations 6 to 9 [7], [12]. The gas rates are added or subtracted from the gas mixtures in the respective volume chambers (cf. Figure 13).

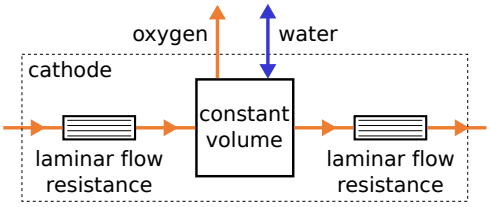

FIG 4. Schematic of the cathode fluid model consisting of a constant volume and two laminar flow resistances

$$\dot{m}_{\mathrm{H_2,\,consumed}} = M_{\mathrm{H_2}} \cdot \frac{NI_{\mathrm{stack}}}{2F} \tag{6}$$

$$\dot{m}_{\mathrm{O_2,\,consumed}} = M_{\mathrm{O_2}} \cdot \frac{NI_{\mathrm{stack}}}{4F} \tag{7}$$

$$\dot{m}_{\mathrm{air}} = M_{\mathrm{air}} \cdot \frac{NI_{\mathrm{stack}}}{0,21 \cdot 4F} \cdot \lambda \tag{8}$$

$$\dot{m}_{\mathrm{H_2O,\,produced}} = M_{\mathrm{H_2O}} \cdot \frac{NI_{\mathrm{stack}}}{2F} \tag{9}$$

Voltage model

The reversible voltage of a fuel cell without losses is described as the Nernst voltage [13]. In order to determine the actual cell voltage, different types of volt-

age losses must be subtracted from this theoretical voltage. The losses can be divided into activation losses, ohmic losses and transport losses. The cell voltage can hence be described as [13]

$$U_{\mathrm{cell}} = E - \Delta U_{\mathrm{act}} - \Delta U_{\mathrm{ohm}} - \Delta U_{\mathrm{trans}}. \tag{10}$$

The Nernst equation can be written as [7], [14]:

$$E = E_0 - \beta(T_{\mathrm{fc}} - T_{\mathrm{ref}}) + \frac{RT_{\mathrm{fc}}}{2F}\left[\ln\left(\frac{p_{\mathrm{H_2}}}{p_{\mathrm{ref}}}\right) + \frac{1}{2}\ln\left(\frac{p_{\mathrm{O_2}}}{p_{\mathrm{ref}}}\right)\right] \tag{11}$$

where

$$\begin{aligned} E_0 &= 1,229\,V, \\ \beta &= 0,85 \cdot 10^{-3}\,\mathrm{V/K}, \\ T_{\mathrm{ref}} &= 298,15\,\mathrm{K}, \\ p_{\mathrm{ref}} &= 1,01325 \cdot 10^5\,\mathrm{Pa}. \end{aligned}$$

E_0 is the potential at reference conditions T_{ref} and p_{ref}, T_{fc} is the operating temperature of the fuel cell, R is the universal gas constant, F is the Faraday constant and $p_{\mathrm{H_2}}$ and $p_{\mathrm{O_2}}$ are the partial pressures of hydrogen and oxygen, respectively.

The activation losses are due to the slowness of the electrochemical reaction, mainly at the cathode side, [14] and can be described according to Larminie et al. [13]:

$$\Delta U_{\mathrm{act}} = \frac{RT}{2\alpha F}\ln\left(\frac{i}{i_0}\right), \tag{12}$$

where α is the charge transfer coefficient, i is the current density and i_0 is the exchange current density. The exchange current density in turn depends on the partial pressure of the reaction gas (here oxygen) $p_{\mathrm{O_2}}$ and the operating temperature T, as described by Barbir [15]:

$$i_0 = i_0^{\mathrm{ref}}\left(\frac{p_{\mathrm{O_2}}}{p_{\mathrm{O_2}}^{\mathrm{ref}}}\right)^{\gamma}\exp\left[-\frac{E_c}{RT}\left(1 - \frac{T}{T_{\mathrm{ref}}}\right)\right] \tag{13}$$

with the pressure coefficient γ and the activation energy for oxygen reduction on the Platinum catalyst E_c. The ohmic losses can be described as [7]:

$$\Delta U_{\mathrm{ohm}} = iR_{\mathrm{ohm,\ total}}. \tag{14}$$

It comprises both membrane resistance and resistance due to the electron transfer through the rest of the cell. However, the electron transfer resistance can be neglected as it is much smaller than the membrane resistance [16]. The membrane resistance can be described as [7]:

$$R_{\mathrm{ohm,\ m}} = \frac{d_{\mathrm{m}}}{\sigma_{\mathrm{m}}} \tag{15}$$

where d_{m} is the membrane thickness and σ_{m} is the membrane conductivity. Springer et al. [17] described the conductivity of a Nafion 117[1] membrane as a function of the operating temperature:

$$\sigma_{\mathrm{m}} = \sigma_{30}\exp\left[1268\,\mathrm{K}\left(\frac{1}{303\,\mathrm{K}} - \frac{1}{T_{\mathrm{cell}}}\right)\right] \tag{16}$$

σ_{30} is the membrane conductivity at a temperature of 30 °C and is a function of the membrane water content λ_{m}. For $\lambda_{\mathrm{m}} > 1$ holds [17], [7]:

$$\sigma_{30} = 0,005139\,\frac{1}{\Omega \cdot \mathrm{cm}} \cdot \lambda_{\mathrm{m}} - 0,00326\,\frac{1}{\Omega \cdot \mathrm{cm}}. \tag{17}$$

For calculation of the membrane water content λ_{m} and water transport through the membrane, please refer to references [7], [17], [18] and [19].

The transport losses are a consequence of the consumption of hydrogen and oxygen which leads to a decline in their partial pressures [13]. According to Larminie et al. [13], an empirical approach to describe the transport loss is given by

$$\Delta U_{\mathrm{Trans}} = m\exp(ni) \tag{18}$$

where the parameters m and n must be well-chosen to provide a good fit.

At last, another small voltage loss occurs due to small amounts of electrons and non-reacted hydrogen molecules passing through the membrane [13]. This effect can be described as an internal leakage current i_n. As described by [9], i_n is added to the external current demand, so that

$$i = \frac{I_{\mathrm{dem}}}{A_{\mathrm{cell}}} + i_n, \tag{19}$$

causing a small shift of the polarization curve towards smaller currents.

Thermal model

According to Macedo-Valencia et al. [20] three different mechanisms contribute to the heat production of a fuel cell stack:
1) chemical reactions,
2) ohmic losses and
3) condensation of water vapor.

Assuming that all reaction water is vaporous, the heat produced due to the chemical reactions and ohmic losses can be determined as follows [12]:

$$\dot{Q}_{\mathrm{react.,\ ohm}} = NI(1.25\,\mathrm{V} - U_{\mathrm{cell}}) \tag{20}$$

where N is the number of cells connected in series and I is the electric current. If the entire chemical energy content of hydrogen was converted into electric energy, the ideal output voltage would be 1.25 V. Hence, the difference between the ideal output volt-

[1] In the experiments described in this publication, no Nafion 117 membrane is used. Due to a lack of available data, however, the model by Springer et al. [17] is used here.

age and the actual output voltage is proportional to the amount of waste heat.

In the event that water condenses within the flow fields, condensation heat is produced which is calculated as follows [6]:

$$\dot{Q}_{\text{cond.}} = \dot{m}_{\text{cond.}} \cdot \Delta h_{\text{H}_2\text{O, evap.}}(T). \tag{21}$$

The produced heat is transferred from the fuel cell stack to the cooling fluid, the reaction gases and the environment. The amount of heat transferred to the individual fluids depends on the respective heat transfer surface A, heat transfer coefficient k and temperature difference ΔT [21]:

$$\dot{Q} = kA\Delta T. \tag{22}$$

4.2. Modeling of peripheral system components

Besides the fuel cell stacks, the investigated system comprises peripheral components including an air blower, valves, a cooling pump and a heat exchanger. The cooling components will not be discussed here. The hydrogen and air subsystem component models will be described in the following.

Air blower

The air blower which provides the air mass flow on the cathode side of the fuel cell stack is modeled via a two-dimensional lookup-table. The lookup-table is based on the blower map which is parameterized by a pressure difference vector, a control voltage vector and a volumetric flow rate matrix. The volumetric flow rate is the linearly interpolated according to the actual pressure difference and control voltage.

Pressure control valves

Different modeling approaches were chosen to model different types of valves. The approach chosen to model the most relevant valve, i.e. the hydrogen pressure control valve, is described in the following.

The hydrogen pressure control valve at the stack inlet is modeled via a volumetric flow rate source. The flow rate is determined via a two-dimensional lookup-table. The lookup-table is defined via a vector of the pressure difference over the valve, a vector of the control current and a volumetric flow rate matrix. Flow rates between the defined entries of the pressure difference and control current vectors are linearly interpolated. The pressure difference is measured across the volumetric flow rate source (cf. Figure 5). The control current is given externally by the pressure controller.

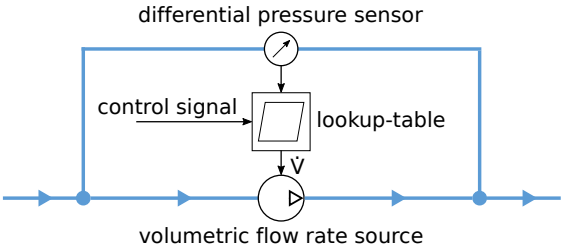

FIG 5. Schematic of the hydrogen pressure control valve model

4.2.1. Approximation of system dynamics

In order to investigate the transient physical system behaviour as well as for the control design (cf. section 5) the model must account for system dynamics. According to Lunze [22] the dynamics of a system with an aperiodically settling transfer function can be approximated by a PT1-Glied. The according transfer function is [22]:

$$f(t) = k_{\text{s}} \left(1 - e^{-\frac{t}{\tau}}\right) \tag{23}$$

where k_s ist the static gain and τ is the time until $f(t) = 0,63$. This approach is chosen to model the dynamics of the air blower, valves, the activation voltage losses and the membrane humidification. The time constants of the activation voltage loss and of the membrane hydration are determined via a parameter estimation (cf. subsection 6.1). All other time constants of system components are either taken from data sheets or estimated manually. The dynamics of the gases are already accounted for within the Simscape modeling language.

5. AUTOMATION OF THE FUEL CELL SYSTEM

Three requirement areas will be covered by the automation. These include the control of the peripheral components, the monitoring of the operating limits and the automated operation of the system. To meet these requirements, on the one hand a superordinate state chart is developed which takes over the tasks of monitoring and automated operation. On the other hand, component controllers are developed, which are used to provide the required operating conditions during the entire operating range. The simplified automation scheme is shown in Figure 6.

5.1. Component control

In order to operate a fuel cell system, it is necessary to provide the required stack operating conditions via the peripheral system components such as pressure valves or compressors as shown in Figure 1. Thus, on the one hand, the provision of a quantity of hydrogen and oxygen required for the reaction and, on the other hand, the setting of an operating temperature are necessary. The control approaches of the peripheral components are described below.

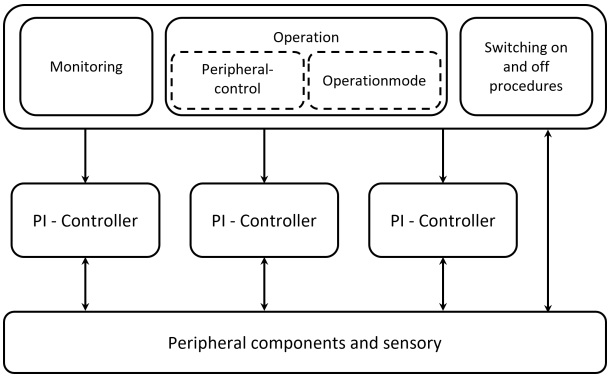

FIG 6. Schematic of the automation architecture of the fuel cell system

Hydrogen pressure control

On the anode side of the fuel cell stack, control of the hydrogen pressure is necessary to maintain a constant hydrogen pressure over the entire operating range. In this way, the hydrogen required for the reaction is provided and hydrogen starvation is avoided at all times. To realize this, the pressure is controlled to a constant value via the proportional valve at the anode inlet using a PI controller. For the model-based controller design, the fuel cell system model is reduced to the components which are relevant for the respective control. The reduced system model used for the design of the hydrogen pressure control is mainly represented by the proportional valve and the anode line within the fuel cell stack. The system under consideration is then linearized. The control parameters are determined via the linearized system within the Simulink Control System Toolbox. Due to a dead time influence in the control, there is currently an oscillation behavior in the hydrogen pressure, which represents a compromise between the control speed and stability of the control. As a result, the hydrogen pressure can only be kept within a band of $\pm 15\,\%$.

Air mass flow control

The air mass flow control is used to provide atmospheric oxygen required for the reaction at the cathode side. The amount of air required is calculated for a defined air ratio λ using Faraday's law according to Equation 8. The air mass flow is controlled by a PI controller and supplied by a radial blower. For the control design, analogously to the hydrogen pressure control, the relevant part of the fuel cell system model is considered, which in this case mainly consists of the air blower and the cathode path within the fuel cell stack. The considered path is linearized at an operating point and the controller is designed using the Simulink Control Systems Toolbox.

Temperature control

The operating temperature also has a major influence on the performance and lifetime of the fuel cell stack. The aim of the operating temperature control is therefore to generate a constant operating temperature which can be specified externally. The coolant mass flow is not variable in the present fuel cell system. Hence, the operating temperature ist controlled mainly via axial fans located on the heat exchanger. Analogously to the control designs described above, the temperature control is also implemented via a PI controller. The P and I parameters are also determined here via the linearized system.

5.2. State chart

The state chart monitors the operating limits, controls the operation itself, and runs defined procedures for switching the system on and off. These are described in detail below.

Monitoring

Within the system monitoring, the operating limits of critical system variables are constantly monitored. In case of exceeding or falling below a respective limit, the system is shut down to avoid possible damages as well as safety-critical conditions.

Start and stop procedures

Each time the fuel cell system is restarted, a start up procedure is completed to ensure that the system starts up safely. Within this start up procedure the peripheral system components are started in a specific sequence so that the required operating conditions are set. The start up procedure of the hydrogen supply contains a leakage check of the hydrogen path during which a defined pressure drop must not be exceeded in order for the system to continue to start up.

Operating modes

On the one hand, there is a manual operating mode which makes it possible to set operating points in the form of current levels and to operate the system as desired. On the other hand, there is an automated operating mode with a defined load profile, which makes it possible to compare the stack performance at different operating conditions or when implementing different control strategies. Parallel to both operating modes, the respective peripheral components are controlled via the control approaches described in subsection 5.1.

5.3. Operation of electrically interconnected stacks in parallel

For parallel operation of the fuel cell stacks, the automation modules and controls are adopted and run in parallel for both stacks. In addition to the operating modes already described, the option of shutting down one of the stacks during manual operation is to be implemented. For parallel operation, both stacks are supplied with the necessary amount of air according to their individual current. Thus, for the theoretical

case where both fuel cell stacks supply the same current at the same voltage, the range of total current available would double. However, to prevent one of the stacks from exceeding the maximum current limit while the other stack is still operating within the allowed range, the individual stack currents are monitored and limited.

In order to be able to adapt the fuel cell system to different load requirements in parallel operation, it is possible to switch individual fuel cell stacks off and on again during operation. This way, the fuel cell stacks can be operated at their optimum power range independently of the load requirement. In this work, a procedure for shutting down and restarting individual fuel cell stacks was developped. A schematic of the chosen procedure is depicted in Figure 7. The amount of air supplied to the stacks is based on the theoretically required amount of air as a function of current and the specified air ratio λ (cf. Equation 8). To shut down one of the stacks while the total current remains the same, the air supply for the other stack is controlled to the amount of air needed to deliver the total current. As soon as the required air supply is reached, the air supply of the other stack is switched off.

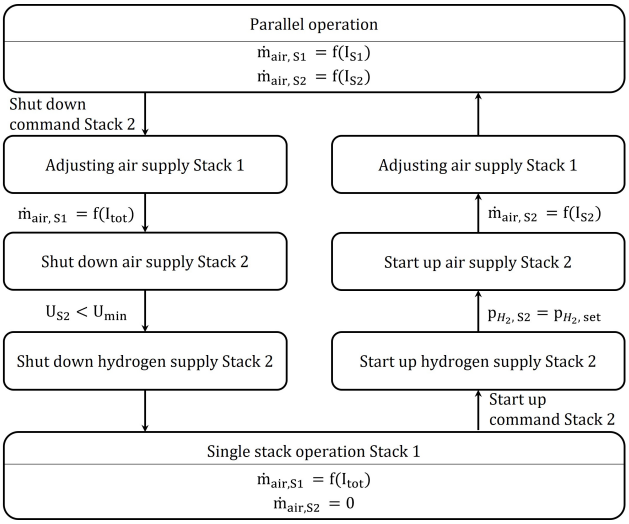

FIG 7. Schematic of the shut down and start up procedure of individual fuel cell stacks during operation

6. RESULTS

In the first part of this chapter, unknown parameters of the developped fuel cell stack model will be fit to experimental data measured at the test rig described in section 3. The outcome of the parameter estimation will also serve as a validation of the stack model. The second part of this chapter shows the parallel operation of fuel cell stacks. The focus is laid on the investigation of the developed shut off and shut on procedure of individual stacks during operation.

Please note that the control design and model improvement and validation did not happen sequentially but rather in an iterative process. Since the controller was needed at an early stage in order to record the shown experimental data, the control design was based on a previous version of the model.

6.1. Voltage model validation

The above described fuel cell system test rig is used to validate different aspects of the fuel cell system model described in section 4. This includes a validation of the stack voltage model as well as the cathode flow resistance.

The stack voltage model is validated via comparison of simulated and measured polarization curves at different temperatures and air ratios. Additionally, the voltage response to a load step input is compared in order to evaluate the correctness of the system dynamics.

As a first step, a parameter estimation is conducted to obtain unknown model parameters. These include the charge transfer coefficient α, the reference exchange current density i_0^{ref}, the initial membrane water content $\lambda_{\mathrm{m,\,init}}$ the hydrogen crossover current density i_n and the transport loss coefficients m and n (cf. section 4) as well as the time constants of the activation loss τ_{act} and of the membrane hydration τ_{m}. Nine different polarization curves at three temperatures and three air ratios were measured at the test rig. Five polarization curves are used for the parameter estimation while the remaining four polarization curves are used for validation of the estimated parameters. Additionally, the voltage response to three different load step inputs are measured. Two sets of measured load step input data are used for the parameter estimation while one set is used for validation of the estimated parameters.

A nonlinear least squares optimization method was used to minimize the voltage error. Time series of the input current, the hydrogen and air volumetric flow rates, the air inlet temperature, the hydrogen inlet pressure and the stack temperature were also recorded at the test rig and feeded to the model. The stack temperature was approximated by the cooling fluid's outlet temperature. The resulting measured and simulated polarization curves are shown in Figures 8 and 9. Small oscillations in the voltage are due to the compromise made regarding the hydrogen pressure controller, as described in section 5.
Please note that the polarization curves were measured continuously at a constant load gradient and are hence not fully stationary. Furthermore, the polarization curves were measured starting from the maximum current demand as it is difficult to maintain the set operating temperature at low currents due to low heat production. For the same reason, the given temperatures could not be maintained throughout the

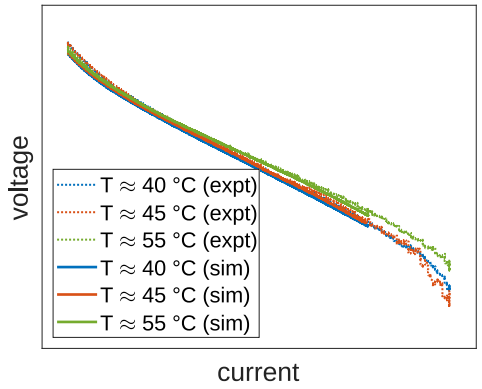

FIG 8. Measured and simulated polarization curves at different temperatures and $\lambda \approx 2.8$.

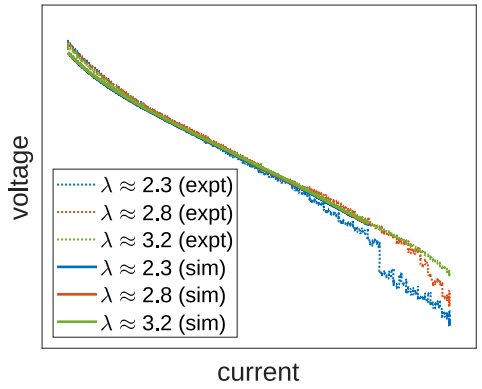

FIG 9. Measured and simulated polarization curves at different air ratios and $T \approx 45°$C.

entire load range. Similarly, the given air ratios could not be maintained throughout the entire load range. At low currents, the air blower reaches its minimum operating point and hence provides a larger air mass flow than necessary. At high currents, on the other hand, the air blower reaches its maximum operating point, causing an undersupply of air.

For the parameter estimation, only the polarization curves' data points up to a certain current density were taken into account, as the voltage partly shows a significant drop at higher current densities (cf. Figure 9, at $\lambda \approx 2.3$). The most probable explanation for the voltage drop is a flooding of the cathode with condensation water due to a small air ratio. Since electrode flooding is not taken into account by the described model, this region is not used for the parameter estimation.

The load step curves, which were also used for the parameter estimation, are not shown here. Please note that the model did not meet the load step curves as well as the polarization curves shown above after the parameter estimation. The model should hence be improved further in the future.

6.2. Fluid model validation

In the fluid model described in section 4, laminar flow was assumed for both ractant gases. Thus, the differential pressure loss was described by Equation 5. This assumption was made as the data measured on the fuel cell system test rig show an almost linear relation between pressure drop and volumetric flow rate of air (cf. Figure 10). This behavior suggests laminar flow within the air flow field rather than turbulent flow, as turbulent flow typically shows a quadratic correlation between pressure drop and volumetric flow rate [23]. In order to meet the measured pressure drop even better, a paremeter estimation for the fluid model shall be conducted in the future. Please note that this validation was only made for the air (cathode) side of the stack. Nevertheless, laminar flow is also assumed on the hydrogen (anode) side here.

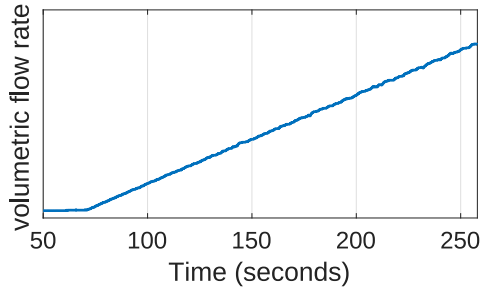

(a) Linearly increasing volumetric flow rate of air

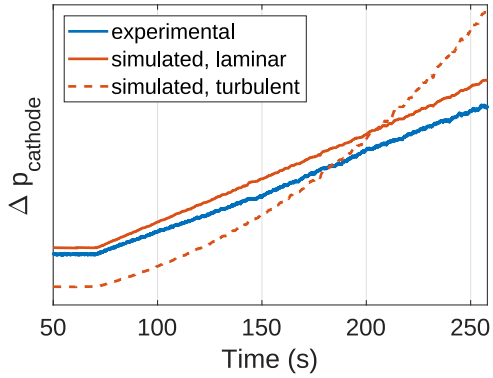

(b) Air pressure difference over the stack's cathode Δp

FIG 10. Comparison of measured cathode pressure drop with simulated laminar and turbulent pressure drops at $T \approx 55\,°$C and $\lambda \approx 2.8$.

6.3. Parallel operation of fuel cell stacks

In the electrical connection of two fuel cell stacks in parallel, the current of both fuel cell stacks adds up to the total current demanded. Figure 11 shows the individual currents and temperatures after the system is switched on from the rest state. Due to performance differences between the fuel cell stacks, there is initially a difference between the currents supplied by the stacks, so that stack 1 provides a larger current than stack 2. Since the reaction takes place exothermically, there is a greater tempera-

ture ascent in stack 1 and the reaction also leads to better humidification of the membrane, so that the performance improves further, while the temperature of stack 1 barely changes due to the low current.

In order to realize a reasonable parallel operation of the stacks, equal or at least similar operating conditions are necessary. In the present work, the fuel cell stacks were first operated individually until a defined operating temperature was reached. Then the system was operated in parallel.

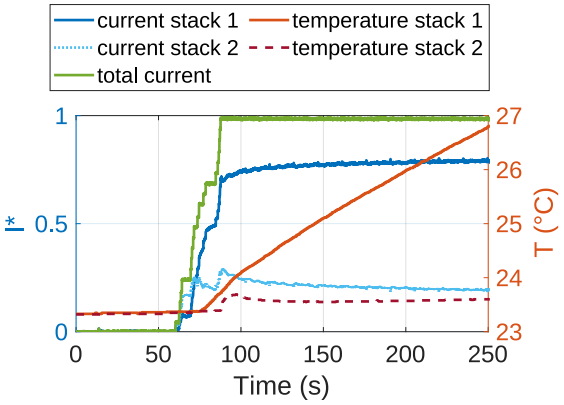

FIG 11. Initial start up with two stacks connected in parallel. Stack 1 provides the majority of the current while stack 2 only provides a very low current. $I^* = I/I_{\text{final}}$ is the normalized current.

Figure 12a shows the total current and the individual currents of the two stacks over time. Both stacks were switched off and on again several times using the developped automation strategy, while the total current remained the same. It can be seen that, compared to Figure 11, the current demand is now much better distributed between the two stacks. Nevertheless, stack 1 provides slightly more current most of the time when both stacks are active.

The process of switching stack 1 off and on again is shown in more detail in Figure 12b. When stack 1 is switched off, the air supply of stack 2 is adjusted to the air requirement for the total current, before the air supply of the stack to be switched off (stack 1) is shut down. This shifts the current towards stack 2 so that a new operating point is established on the single stack characteristic. By switching off one of the stacks at a constant total current demand, a new voltage is set (cf. Figure 12c). Due to the voltage drop at the diodes, which are installed behind the stacks, a diverging voltage occurs at the switched-off stack. In order to maintain a constant output voltage, the total current demand would also have to be adjusted accordingly when switching individual stacks on and off.

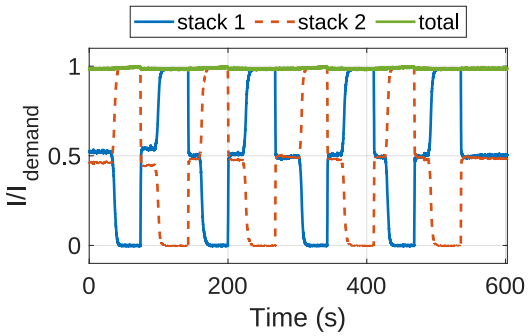

(a) Currents of the two stacks

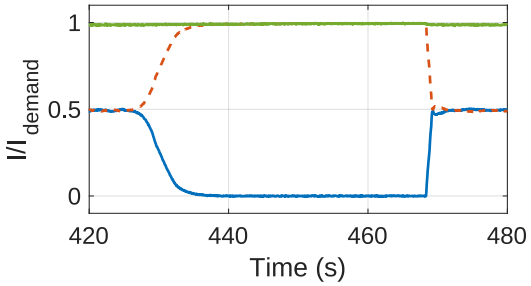

(b) Zoom of the currents

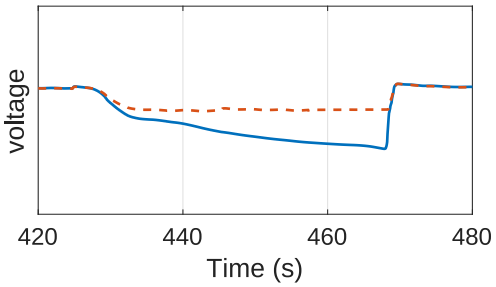

(c) Zoom of the voltages

FIG 12. Currents and voltages of the two stacks which are alternately switched off and on again.

7. CONCLUSION

Within the presented work, an automation strategy for parallel operation of fuel cell stacks is developped. First, different interconnection types of fuel cell stacks and the respective advantages and disadvantages are discussed. For the experimental investigation of the developped automation strategy, a scaled fuel cell system test rig including two fuel cell stacks interconnected in parallel is built up. The development of the automation strategy itself is based on a system model representing the test rig. This model is developed using a physical network modeling approach. The focus is laid on representing transient effects depending on operating conditions such as temperatures, pressures and reactant gas humidities. Following, the model is used for the design of PI-controllers for all controllable components. A superordinate state chart runs predefined start up and shut down procedures, enables the controllers and monitors critical system states. The model and controllers were iteratively improved using the fuel cell system test rig. The

measured data is used for the fuel cell stack model to undergo a parameter estimation using a nonlinear least squares optimization method. The result also serves as a model validation. Eventually, the start up and shut down procedure during operation of individual stacks interconnected in parallel is demonstrated.

Within the scope of following research works, the controllers can be further improved. Especially the hydrogen pressure control loop still shows some oscillations which shall be removed in order to realize stationary conditions. Regarding further improvements of the model, another parameter estimation could be done for the stack's fluid model as well as for peripheral system components. Also, the validation can be extended to a wider range of operating conditions. In terms of the parallel interconnection of fuel cell stacks, further testing shall be conducted including a load change when switching individual stacks off and on again. One possible control target is to keep the voltage of the stack remaining active nearly constant. In this way, possible degradation due to unnecessary load changes shall be minimized.

Contact address:

sebastian.nicolay@mtu.de

ACKNOWLEDGEMENTS

The research work associated with this publication has been supported by the German Federal Ministry for Economic Affairs and Climate Action under grant number 20M1908H. The funding of the work through the 1st call of the Federal Aviation Research Program VI (LuFo VI-1), grant project title 'E-SATstart', is gratefully acknowledged.

References

[1] Hepperle, M.: "Electric Flight - Potential and Limitations". In: *Energy Efficient Technologies and Concepts of Operation*. Oktober 2012.

[2] Barbir, F.: "CHAPTER 6 - Stack Design". In: *PEM Fuel Cells*. Ed. by Barbir, F. Burlington: Academic Press, 2005, pp. 147–206. ISBN: 978-0-12-078142-3. DOI: https://doi.org/10.1016/B978-012078142-3/50007-0.

[3] Schefer, H., Fauth, L., Kopp, T. H., et al.: "Discussion on Electric Power Supply Systems for All Electric Aircraft". In: *IEEE Access* 8 (2020), pp. 84188–84216. DOI: 10.1109/ACCESS.2020.2991804.

[4] Department of Defense: *MIL-STD-704F. Aircraft Electric Power Characteristics*. Interface Standard. Mar. 12, 2004.

[5] The MathWorks, Inc.: *Simscape™ User's Guide (R2021a)*. 2021. URL: https://de.mathworks.com/help/pdf_doc/physmod/simscape/index.html (visited on 07/06/2021).

[6] The MathWorks, Inc.: *Constant Volume Chamber (MA)*. 2022. URL: https://de.mathworks.com/help/physmod/simscape/ref/constantvolumechamberma.html (visited on 09/01/2022).

[7] Pukrushpan, J.: "Modeling and Control of Fuel Cell Systems and Fuel Processors". Dissertation. The Uniersity of Michigan, Jan. 2003.

[8] Gößling, S., Beckhaus, P., and Heinzel, A.: "Dynamic PEMFC Model as a Base for a State Classifier and Controller". In: *Energy Procedia* 28 (2012). Fuel Cells 2012 Science & Technology – A Grove Fuel Cell Event, pp. 113–124. ISSN: 1876-6102. DOI: https://doi.org/10.1016/j.egypro.2012.08.045.

[9] Gößling, S.: "2-D + 1-D ortsaufgelöste Modellierung von PEM-Brennstoffzellen". Dissertation. Universität Duisburg-Essen, Mar. 2019, pp. 54–55. ISBN: 978-3-8439-4032-0.

[10] The MathWorks, Inc.: *PEM Fuel Cell System*. 2021. URL: https://de.mathworks.com/help/physmod/simscape/ug/pem-fuel-cell-system.html (visited on 08/30/2022).

[11] PFITZNER, J.: "Poiseuille and his law". In: *Anaesthesia* 31(2) (1976), pp. 273–275. DOI: https://doi.org/10.1111/j.1365-2044.1976.tb11804.x. eprint: https://associationofanaesthetists-publications.onlinelibrary.wiley.com/doi/pdf/10.1111/j.1365-2044.1976.tb11804.x.

[12] Larminie, J. and Dicks, A.: "Appendix 2: Useful Fuel Cell Equations". In: *Fuel Cell Systems Explained*. John Wiley & Sons, Ltd, 2003, pp. 395–400. ISBN: 9781118878330. DOI: https://doi.org/10.1002/9781118878330.app2. eprint: https://onlinelibrary.wiley.com/doi/pdf/10.1002/9781118878330.app2.

[13] Larminie, J. and Dicks, A.: "Operational Fuel Cell Voltages". In: *Fuel Cell Systems Explained*. John Wiley & Sons, Ltd, 2003. Chap. 3, pp. 45–66. ISBN: 9781118878330. DOI: https://doi.org/10.1002/9781118878330.ch3. eprint: https://onlinelibrary.wiley.com/doi/pdf/10.1002/9781118878330.ch3.

[14] Amphlett, J. C., Baumert, R. M., Mann, R. F., et al.: "Performance Modeling of the Ballard Mark IV Solid Polymer Electrolyte Fuel Cell: I . Mechanistic Model Development". In: *Journal of The Electrochemical Society* 142(1) (Jan. 1995), pp. 1–8. DOI: 10.1149/1.2043866.

[15] Barbir, F.: "CHAPTER 3 - Fuel Cell Electrochemistry". In: *PEM Fuel Cells*. Ed. by Barbir, F. Burlington: Academic Press, 2005, pp. 33–72. ISBN: 978-0-12-078142-3. DOI: https://doi.org/10.1016/B978-012078142-3/50004-5.

[16] Ceraolo, M., Miulli, C., and Pozio, A.: “Modelling static and dynamic behaviour of proton exchange membrane fuel cells on the basis of electro-chemical description”. In: *Journal of Power Sources* 113(1) (2003), pp. 131–144. ISSN: 0378-7753. DOI: https://doi.org/10.1016/S0378-7753(02)00565-7.

[17] Springer, T. E., Zawodzinski, T. A., and Gottesfeld, S.: “Polymer Electrolyte Fuel Cell Model”. In: *Journal of The Electrochemical Society* 138(8) (Aug. 1991), pp. 2334–2342. DOI: 10.1149/1.2085971.

[18] Dutta, S., Shimpalee, S., and Van Zee, J.: “Numerical prediction of mass-exchange between cathode and anode channels in a PEM fuel cell”. In: *International Journal of Heat and Mass Transfer* 44(11) (2001), pp. 2029–2042. ISSN: 0017-9310. DOI: https://doi.org/10.1016/S0017-9310(00)00257-X.

[19] Nguyen, T. V. and White, R. E.: “A Water and Heat Management Model for Proton-Exchange-Membrane Fuel Cells”. In: *Journal of The Electrochemical Society* 140(8) (Aug. 1993), pp. 2178–2186. DOI: 10.1149/1.2220792.

[20] Macedo-Valencia, J., Sierra, J., Figueroa Ramirez, S., et al.: “Numerical study of heat transfer in a PEM fuel cell with different flow-fields”. In: XV International Congress of the Mexican Hydrogen Society Mexico, D.F. 2015. Nov. 2015.

[21] The MathWorks, Inc.: *Convective Heat Transfer*. 2022. URL: https://de.mathworks.com/help/physmod/simscape/ref/convectiveheattransfer.html (visited on 09/05/2022).

[22] Lunze, J.: “Verhalten linearer Systeme”. In: *Regelungstechnik 1: Systemtheoretische Grundlagen, Analyse und Entwurf einschleifiger Regelungen*. Berlin, Heidelberg: Springer Berlin Heidelberg, 2020, pp. 123–233. ISBN: 978-3-662-60746-6. DOI: 10.1007/978-3-662-60746-6_5.

[23] Böswirth, L. and Bschorer, S.: “Rohrströmung und Druckverlust”. In: *Technische Strömungslehre: Lehr- und Übungsbuch*. Wiesbaden: Springer Fachmedien Wiesbaden, 2014, pp. 177–216. ISBN: 978-3-658-05668-1. DOI: 10.1007/978-3-658-05668-1_8.

APPENDIX

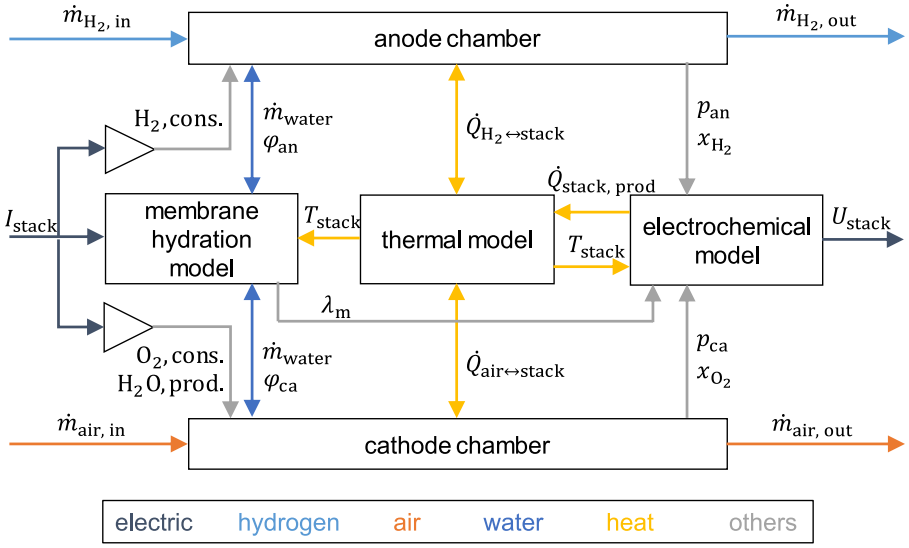

FIG 13. Schematic of the fuel cell stack model including submodels and major interactions